Numerical investigation on the influence of inclusion shape on concrete drying shrink- age fracture behavior

Yu SUN , Jean-Philippe CARLIER, Thomas ROUGELOT, Yun JIA

Univ. Lille, CNRS, Centrale Lille, UMR 9013 - LaMcube - Laboratoire de Mécanique, Multiphysique, Multi-échelle, F-59000 Lille, France

ABSTRACT

The characteristics of inclusions have a great influence on the fracture characteristics of concrete. In this research paper, a numerical investigation on the influence of inclusion shape on concrete shrinkage fracture behavior is presented. A meso-scale finite element model of concrete is established, considering the three-phase composite structure of inclusions, mortar, and interfacial transition zone (ITZ). An elastic-plastic damage model is used to describe the mechanical behavior of the mortar under drying conditions, while the inclusions are assumed to be elastic. A humidity diffusion model is coupled with the mechanical model to simulate the moisture transport and the shrinkage strain in the concrete. The paper analyzes the effects of different inclusion shapes, such as circular, elliptical, and polygonal, on the crack initiation and propagation in concrete. The results show that the inclusion shape has a significant impact on stress concentration, crack pattern, and crack area of concrete. The paper provides theoretical insights for the prevention and treatment of concrete shrinkage cracks.

Keywords concrete, finite element method, elastic-plastic damage model, drying shrinkage, fracture characteristics

I. Introduction

Concrete is a fundamental material in modern society, widely applied in diverse engineering applications such as constructing buildings and establishing nuclear plants. Cracks in concrete pose a substantial threat to its structural integrity and durability, potentially leading to severe consequences (Mehndi et al. 2014). Therefore, it is crucial to gain a comprehensive understanding of the causes and mechanisms of concrete cracking to facilitate effective design and maintenance of concrete structures.

Among the many factors affecting concrete cracking, drying shrinkage plays an important role. The drying shrinkage of concrete can be attributed to four primary mechanisms. These mechanisms include the change in surface free energy of the solid phase, capillary tension effect leading to equal hydrostatic compression in the solid phase, changes in the disjoining pressure in areas of hindered adsorption, and the movement of interlayer water (Almudaiheem 1991). The inclusions mixed with cement and water play a critical role in concrete properties. These properties include strength, thermal and elastic characteristics, dimensional and volume stability, and overall durability (Sáez-Pérez et al. 2020, Talaat et al. 2021).

In this paper, a finite element meso-scale model of concrete in dry environment was established, and an elastic-plastic damage model of concrete was calibrated. Through this simulation, the influence of inclusion shape on the drying shrinkage cracks of concrete at meso-scale was studied. This study can provide theoretical reference for the prevention and treatment of concrete dry shrinkage cracks.

II. Hydro-mechanical coupling finite element model for concrete

Comprehending the evolution of internal humidity gradients within concrete over time is vital for analyzing the propagation of cracks. This study focuses on elucidating the mechanism of drying shrinkage cracks in concrete under relatively dry conditions, adopting a meso-scale perspective that specifically delves into surface-level drying shrinkage cracks. Concrete is conceptualized in this study as a three-phase composite material, comprising inclusions, mortar, and interfacial transition zone (ITZ) (Xu & Chen 2016). The research involves numerical simulations to investigate the propagation of drying shrinkage cracks in concrete specimens subjected to dry conditions.

A. Humidity diffusion model

It is generally believed that the diffusion of water in concrete satisfies Fick's second law (Zhou et al. 2020). And the diffusion of water in concrete is considered as the change of humidity field. Ignoring the influence of temperature and self-shrinking, the governing equation of the transient humidity field is:

$$\frac{\partial h}{\partial t} = \operatorname{div}\left[D\left(h\right) \cdot \operatorname{grad}\left(h\right)\right] \tag{1}$$

where h is the relative humidity, $D(h)$ is the water diffusion coefficient. The convection boundary conditions on the cement surface is considered as (Martinola 1995):

$$q_s = H_F \cdot (h_s - h_a) \tag{2}$$

where q_s is the wet flux perpendicular to the concrete surface; H_F is the surface humidity exchange coefficient; h_s is the relative humidity of the concrete surface; h_a is the environmental relative humidity.

According to the humidity diffusion equation, the moisture diffusion in concrete depends on the humidity diffusion coefficient of different materials, and the humidity diffusion coefficient has a strong correlation with the current humidity. Previous studies combined the inversion of the humidity diffusion equation with the least square method to determine the law of the humidity diffusion coefficient (Wittmann et al. 1989), which was described by the exponential equation:

$$D_m(h) = 0.22e^{5.4h}(\mathrm{mm}^2/\mathrm{day}) \tag{3}$$

where D_m is the humidity diffusion coefficient of cement paste, the humidity diffusion coefficient of inclusion is 1/50 of that of cement paste (Bolander Jr & Berton 2004). The strain field can be calculated from the distribution of the humidity field according to the following (Yang et al. 2017):

$$\dot{\varepsilon}_{ij}^{h} = \alpha_{sh} \cdot \dot{h} \tag{4}$$

where $\dot{\varepsilon}_{ij}^{h}$ is the dry shrinkage strain; α_{sh} is the shrinkage coefficient; $\dot{h}$ is the humidity gradient.

In this simulation, the inclusion is set as an elastic model, and the mortar is used the elastic-plastic damage constitutive to describe the fracture behavior.

The elastic-plastic model is established for simplicity and emphasizes the hydro-mechanical behavior of the concrete during drying. With the assumption of small deformations and small perturbations, the strain caused by hydraulic gradient ε_{ij}^{h} is decomposed into an elastic part ε_{ij}^{e} and plastic one ε_{ij}^{p}

$$\varepsilon_{ij}^{h} = \varepsilon_{ij}^{e} + \varepsilon_{ij}^{p} \tag{5}$$

The stress tensor (stresses in the undamaged mortar) can be written in terms of the strain equivalence hypothesis and using Hooke's law as:

$$\sigma'_{ij} = E'_{ijkl}\varepsilon^e_{kl} = E'_{ijkl}(\varepsilon^h_{kl} - \varepsilon^p_{kl}) \tag{6}$$

where E'_{ijkl} is the fourth-order isotropic elasticity tensor, also known as the elastic modulus of undamaged mortar. The rate of the stress tensor in the effective (undamaged) configuration can be written in terms of the strain equivalence hypothesis and Hooke's law as:

$$\dot{\sigma'}_{ij} = E'_{ijkl}\dot{\varepsilon}^e_{kl} = E'_{ijkl}(\dot{\varepsilon}^h_{kl} - \dot{\varepsilon}^p_{kl}) \tag{7}$$

B. Damage model

When the damage is introduced into the model, the stress tensor for the damaged material, is given as follows:

$$\sigma_{ij} = E_{ijkl}(\omega)\varepsilon^e_{kl} = E_{ijkl}(\omega)(\varepsilon^h_{kl} - \varepsilon^p_{kl}) \tag{8}$$

where E_{ijkl} is the fourth-order elasticity tensor dependent on the damage properties. Applying the effective stress concept, the Cauchy stress tensor σ_{ij} is related to the effective stress tensor σ'_{ij} through the following expression:

$$\sigma_{ij} = (1-\omega)\sigma'_{ij} \tag{9}$$

For the sake of simplicity and convenience, the current study employs an isotropic damage model, conveniently described by a scalar variable ω denoted as

$$\omega = (1-\alpha_t)\omega_c + \alpha_t\omega_t; \alpha_t = \frac{\|{\sigma_{ij}}^+\|}{\|\sigma_{ij}\|} \tag{10}$$

where ω_c represents the compression damage parameter; ω_t represents the tension damage parameter; α_t is the ratio of tensile stresses with respect to total stresses; $\|{\sigma_{ij}}^+\|$ and $\|\sigma_{ij}\|$ are respectively the norm of total stress tensor σ_{ij} and that of tensile stress tensor ${\sigma_{ij}}^+$. For uniaxial compression test α_t = 0 while α_t = 1 in uniaxial tensile test. So the effective elastic modulus of damaged concrete can be defined by the relations:

$$E_{ijkl} = (1-\omega)E'_{ijkl} \tag{11}$$

and the incremental form of the constitutive equation can be expressed as follows:

$$\dot{\sigma}_{ij} = E_{ijkl}\dot{\varepsilon}^e_{kl} - E'_{ijkl}\varepsilon^e_{kl}\dot{\omega} \tag{12}$$

On the basis of the experimental data and inspired by the damage model used by some previous works (Bian et al. 2016) and (Mazars & Pijaudier-Cabot 1989), the following criteria are proposed for the evolution of tensile damage and compressive damage.

$$\begin{aligned} \varepsilon_{eq} &= 2\sqrt{\sum_{i=1}^{3}\langle\varepsilon_{ii}\rangle^2} \\ \gamma^p &= \int\sqrt{\tfrac{2}{3}\dot{e}^p_{ij} : \dot{e}^p_{ij}}; \dot{e}^p_{ij} = \dot{\varepsilon}^p_{ij} - \tfrac{tr(\dot{\varepsilon}^p_{ij})}{3}\delta_{ij} \end{aligned} \tag{13}$$

where ε_{ii} is the ith principal strain, and the bracket $\langle\varepsilon_i\rangle$ means that only the positive value is taken into account; γ^p is the generalized plastic shear strain; δ_{ij} is the second order unit tensor. Therefore, the following criteria are proposed for the evolution of tensile damage and compressive damage.

$$F_{\omega_t} = 1 - \frac{1}{\exp(B_t \varepsilon_{eq})} - \omega_t \leq 0 \tag{14}$$

$$F_{\omega_c} = 1 - \frac{1}{\exp(B_c \gamma^p)} - \omega_c \leq 0 \tag{15}$$

where B_c controls the kinetics of compressive damage $\omega_c$and B_t characterizes the evolution of tensile damage ω_t.

C. *Elastic-plastic model*

In order to account for the high dependence of containment pressure on plastic behaviour, a non-linear loading surface is usually required. Inspired by the earlier work of Zhou et al. (2013), a yield surface is used for cement materials:

$$F_p(\sigma_{ij}, \gamma^p, \omega) = q - \alpha(\gamma^p) \left(-{c_1}^2 + \sqrt{{c_1}^2 + 4c_2(c_3 - \frac{p}{f_c\,(\omega)})} \right) \frac{f_c(\omega)}{c_2} = 0 \tag{16}$$

where three parameters c_1, c_2, c_3 define the pattern of the yield surface, and can be calibrated by experimental data (Table 1), as shown in Figure 1; p is the mean effective stress and q denotes the deviatoric effective stress. To describe the impact of damage on mechanical strength, we assume a reduction in the uniaxial compression strength of concrete as damage occurs. For simplicity, the following linear relation is proposed:

$$f_c(\omega) = \left(1 - \frac{\langle \omega - \omega_0 \rangle}{1 - \omega_0} \right) f_{c0} \tag{17}$$

where ω_0 is the damage value at the level of peak stress; f_{c0} is the uniaxial compression strength f_c of undamaged cement.

Table 1: Triaxial test results of concrete under different confining pressures

Confining pressure (MPa)	Peak deviatoric stress (MPa)	Strain corresponding with peak stress
0	48	0.011
5	56.4	0.017
10	65	0.055
20	84	0.066

The evolution of the yield surface is governed by the plastic hardening law, which amplifies with the generalized plastic shear strain, denoted as γ^p. Utilizing representative experimental data, the following plastic hardening law is employed:

$$\alpha(\gamma^p) = 1 - \exp(-\xi \gamma^p) \tag{18}$$

The law of plastic work hardening α varies from 0 to 1. The fracture surface is reached when $\alpha \to 1$. The parameter ξ controls the kinetics of plastic work hardening. As many experimental results have shown, a compaction/dilatation transition with the increase of the deviatorical stress was noticed. It is then necessary to choose an unassociated law, choosing an adequate plastic potential. Among the various existing models, the following plastic potential is adopted (Jia et al. 2010):

$$Q_p\left(\sigma_{ij}, \gamma^p, \omega\right) = q - \eta(-p + c_3 f_c(\omega)) \ln \left(\frac{-p + c_3 f_c\,(\omega)}{I_0} \right) = 0 \tag{19}$$

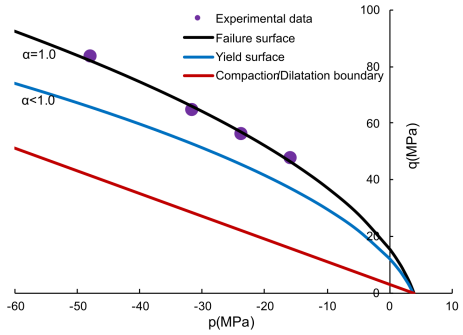

FIGURE 1. The failure surface calibrated by experimental data, yield surface and compaction/dilatation boundary

where the variable I_0 is the current intersection of the plastic potential and the p axis. The boundary between the field of compaction and dilatation is defined by the condition $\partial Q_p/\partial p = 0$, which is expressed as follows:

$$F_s = q - \eta(-p + c_3 f_c(\omega)) = 0 \tag{20}$$

The parameter η defines the slope of the boundary between compaction and dilatation domain in the p-q plan.

Under general loading conditions, plasticity and damage are coupled. For this reason, it is necessary to define the evolution of plastic deformation and damage. A coupled algorithm is then necessary at each material point to determine the evolution of plastic deformation and damage. However, since damage is related to total deformation in the proposed model, damage evolution can be determined first at the beginning of each stage. A simplification is adopted for the loading coefficient α_t and the damage parameter ω, which are calculated from the stress and the plastic shear strain obtained at the end of previous step. Then the classic algorithm of plastic correction is used. The plastic multiplier $\dot{\lambda}_p$ is determined by the plastic consistency condition:

$$\frac{\partial F_p}{\partial \sigma_{ij}} d\sigma_{ij} + \frac{\partial F_p}{\partial \gamma^p} d\gamma^p + \frac{\partial F_p}{\partial \omega} d\omega = 0 \tag{21}$$

$$\dot{\lambda}_p = \frac{\frac{\partial F_p}{\partial \sigma_{ij}} : E_{ijkl}(\omega) d\varepsilon_{kl} - \frac{\partial F_p}{\partial \sigma_{ij}} : E'_{ijkl} \varepsilon^e_{ij} d\omega + \frac{\partial F_p}{\partial f_c} \frac{\partial f_c}{\partial \omega} d\omega}{\frac{\partial F_p}{\partial \sigma_{ij}} : E_{ijkl}(\omega) : \frac{\partial Q_p}{\partial \sigma_{ij}} - \frac{\partial F_p}{\partial \alpha_p} \frac{\partial \alpha_p}{\partial \gamma^p} \left(\frac{\partial \gamma^p}{\partial \varepsilon^p_{ij}} : \frac{\partial Q_p}{\partial \sigma_{ij}} \right)} \tag{22}$$

To simplify calculations, the creep behavior of cement paste has not been taken into account. The model proposed in this paper is implemented using UMAT in the finite element software ABAQUS. In the UMAT, at each step, an increment of total deformation is given at each point (Figure 2). The corresponding increases in stress, plastic strain and damage are calculated using the equations and loading conditions. After a trivial elastic prediction, the plasticity and damage criteria are checked according to loading conditions.

III. Calibration of proposed model and boundary condition

In this section, the proposed model is applied to study the mechanical behavior of concrete under a wide range of confining pressure. The cement used is a Portland cement CEM II/B 32.5R and the paste has a water to cement ratio W/C equal to 0.5 (Li 2016). The model's parameters calibrated by the experimental data is shown in Table 2.

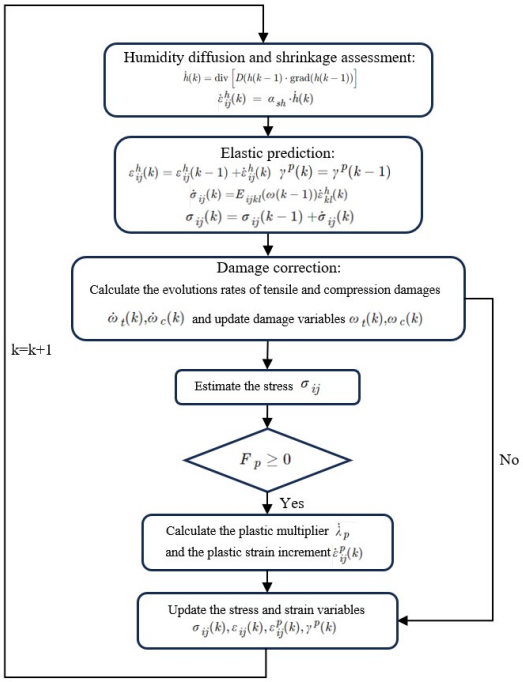

FIGURE 2. Flow chart for numerical implementation of hydro-mechanical model at the kth step

A. Calibration of proposed model

To test the model's ability to reproduce the mechanical behaviour of cement paste, one uniaxial tensile test and four triaxial compression tests with different confining pressures are simulated using the specified parameters. The simulation results are presented in Figure 3. In general, a good agreement is obtained between the numerical simulations and the experimental data. Therefore, the proposed model is able to satisfactorily describe the main characteristics of the behavior of the cement material.

B. Meso-scale model and boundary condition

In order to ensure the speed of calculation, 2D simulation is used in this calculation. The size of the finite element model is 12 mm×12 mm and the 4-node plane strain thermally coupled displacement and temperature element type is used. After a mesh size sensitivity analysis, the crack can be well characterized with a mesh precision of 0.05mm, and the total number of element is then 57600. The effect of the mesh is minimized by dividing different areas on the uniform mesh. This model is divided into three parts: cement, inclusion and ITZ. The shrinkage coefficient of cement paste is 0.7‰ (Zhou et al. 2020). The parameter of humidity of cement and ITZ were set to the same value. Previous studies have shown that, the elastic modulus of ITZ is 50% to 70% of the elastic modulus of cement paste, and the strength is 30% to 50% of the strength of cement paste (Liao et al. 2004). In this study, the interface tensile strength was taken as 40% of the strength of cement paste, and the elastic modulus of ITZ was taken as 60% of the elastic modulus of cement paste. We assumed that the inclusion shrinkage coefficient is 0.

In order to study the effect of inclusion shape on concrete cracking, inclusions were randomly placed in the mesh, the volume fraction of these inclusions being set at 40%. Inclusions with different shapes were

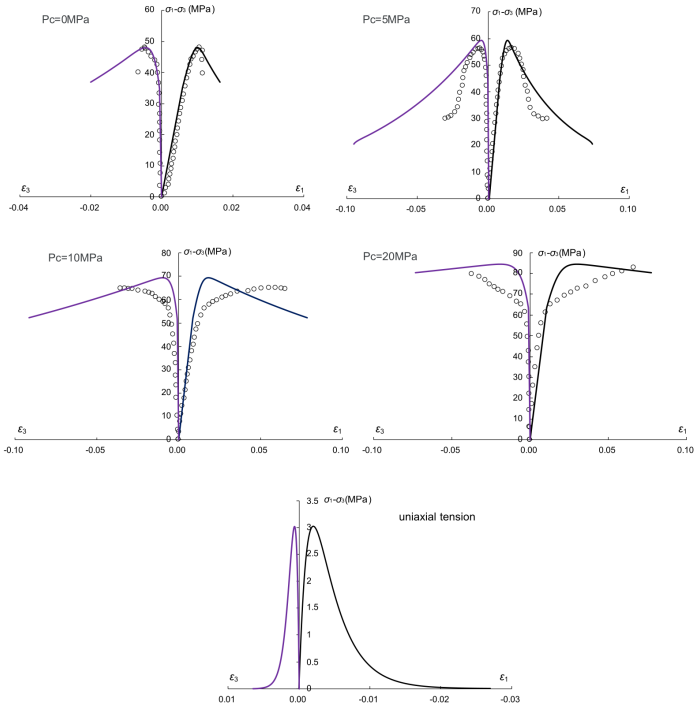

FIGURE 3. Comparison of numerical simulation (continuous lines) and test data (points)

then placed in the same spatial position to reduce the influence of the spatial distribution of inclusions on the simulation results (Figure 4). In the humidity diffusion simulation, the initial relative humidity of concrete is set to 1. The surface humidity exchange condition is set at the four edges of the model. The surface humidity exchange coefficient (H_F) is 1.5 mm/day (Zhou et al. 2020), and the relative humidity in the external dry environment is set to 0.45. In the wet stress simulation, a displacement constraint in the X and Y direction was applied at the center point of the model, and a predefined humidity field was set. The drying process was simulated during 30 days.

TABLE 2. Parameters used in the simulation

E(GPa)	v	η	f_{c0}(MPa)	c_1	c_2	c_3	ξ	B_t	B_c
6	0.25	0.8	45	0.16	1.1	0.08	800	150	20

C. Simulation result

Studying the variation of concrete humidity field, especially at the surface of concrete, can lead to a better understanding of the evolution law of dry shrinkage cracks. Three typical change points of the concrete are selected for analysis, which are the corner point of the model, the middle point of the side edge of the test block and the center point of the model. Figure 5 shows the humidity change curve of the three selected points with drying time. Among them, the moisture at the corner point and the middle point of the edge of the test block rapidly decreased and tended to be stable within t=5 days, close to the humidity of 0.45. This is due to the existence of two and one convective surface at the corner and edge respectively, which accelerate

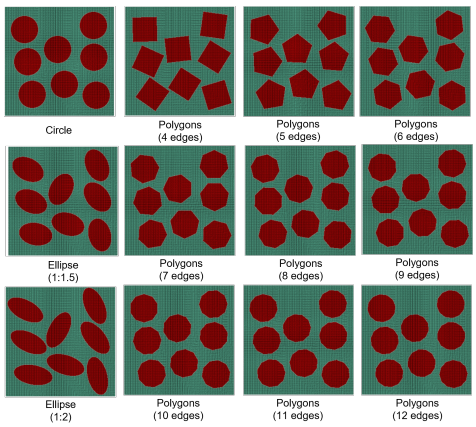

FIGURE 4. The models with different shape inclusions

the diffusion of water. And the relative humidity RH=0.45 is reached when t=30 day. As the center of the model is far from the dry boundary, the humidity drops slowly. When t=30 day, the relative humidity RH is 0.47. It can be seen that the convection boundary conditions between concrete and dry environment have a great influence on the water diffusion rate and humidity distribution of concrete.

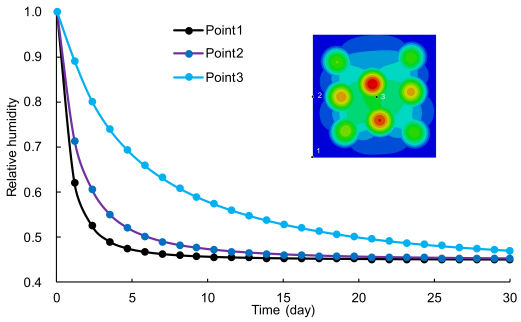

FIGURE 5. Humidity field simulation result (Circle inclusions model represented; three points from outside to inside as representative points)

The simulation results of the damaged field of the concrete shown in the Figure 6 show that when the concrete with different shape inclusions are subjected to the same drying conditions, the degree of damage is very different. For circular inclusions, the location of cracks is within the ITZ. In contrast, when considering elliptical inclusions, those with larger aspect ratios tend to induce more extensive and prolonged cracking within the concrete matrix. The elongated shape exacerbates stress concentration, thereby promoting crack propagation.

In Figure 6, it's notable that cracks predominantly occur at the corners of polygonal inclusions. It shows that the cracks are related to the angle of polygonal inclusions corners. According to the constitutive model, the elements with a damage value greater than 0.6 are considered to be crack locations. As shown in the Figure 7, the angle of inclusions corners has a great influence on the maximum principal stress and the maximum principal strain of the whole model. And the crack area exhibits a notable decrease as the angle of inclusion corners increases ; the influence threshold of angle on crack area being 120°. There is a high correlation between the trend of the maximum principal stress and the crack area. This phenomenon indicates

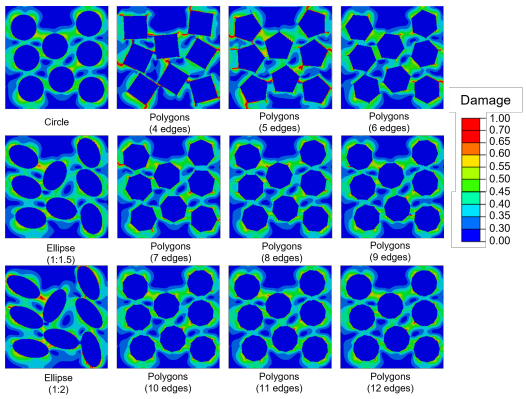

FIGURE 6. Damaged field simulation result of the models with different shape inclusions

that, compared with blunter corners, sharp corners concentrate stress more effectively and exacerbate crack propagation. Therefore, polygon inclusions with rounded corner are less likely to generate extensive cracks in the concrete drying process.

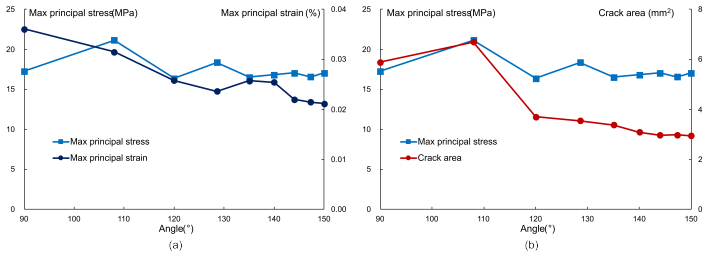

FIGURE 7. Crack area evolution of the models with different shape inclusions

IV. Discussion

This paper investigates and analyzes the influence of the inclusion shape on the fracture properties of concrete under drying conditions. Experimental data in the literature were used to verify the applicability of the elastic-plastic damage model, then the model was used to analyze the cracking characteristics of concrete under dry conditions from the perspective of inclusion shape. The conclusions drawn from this study are summarized as below:

1. The proposed elastic-plastic damage model can satisfactorily describe the main characteristics of the mechanical behavior of concrete under various confining pressures. Moreover, by combining it with the humidity diffusion model, the model can well simulate the cracking patterns of concrete under drying condition.

2. The inclusion shape has a significant influence on the fracture behavior of concrete under drying conditions, with circular inclusions being the most favorable for crack resistance. The aspect ratio of elliptical inclusions affects the stress concentration and crack propagation in the concrete matrix, with higher aspect ratios leading to more extensive and prolonged cracking.

3. The angle of polygonal inclusions corners also affects the crack initiation and development, with sharper angles inducing more stress concentration and crack area. The influence threshold of angle on crack area is 120°.

The study provides theoretical reference for the prevention and treatment of concrete dry shrinkage cracks and suggests that the inclusion shape should be considered in the design and optimization of concrete materials.

References

Almudaiheem, J. A. (1991), 'Prediction of drying shrinkage of portland cement paste: Influence of shrinkage mechanisms', *Journal of King Saud University - Engineering Sciences* **3**(1), 69–86.

Bian, H., Jia, Y., Shao, J. & Pontiroli, C. (2016), 'Numerical study of a concrete target under the penetration of rigid projectile using an elastoplastic damage model', *Engineering Structures* **111**, 525–537.

Bolander Jr, J. E. & Berton, S. (2004), 'Simulation of shrinkage induced cracking in cement composite overlays', *Cement and Concrete Composites* **26**(7), 861–871.

Jia, Y., Bian, H., Su, K., Kondo, D. & Shao, J.-F. (2010), 'Elastoplastic damage modeling of desaturation and resaturation in argillites', *International journal for numerical and analytical methods in geomechanics* **34**(2), 187–220.

Li, L. (2016), Etude de la fissuration engendrée par le séchage dans les matériaux cimentaires: influence des inclusions, PhD thesis, École doctorale Sciences pour l'ingénieur (Lille).

Liao, K.-Y., Chang, P.-K., Peng, Y.-N. & Yang, C.-C. (2004), 'A study on characteristics of interfacial transition zone in concrete', *Cement and Concrete research* **34**(6), 977–989.

Martinola, G. (1995), 'Application of fracture mechanics to optimize repair mortar system', *Fracture Mechanics of Concrete Structures* pp. 1481–1492.

Mazars, J. & Pijaudier-Cabot, G. (1989), 'Continuum damage theory—application to concrete', *Journal of engineering mechanics* **115**(2), 345–365.

Mehndi, S. M., Khan, M. & Ahmad, S. (2014), 'Causes and evaluation of cracks in concrete structures', *International Journal of Technical Research and Applications* **2**(5), 29–33.

Sáez-Pérez, M. P., Brümmer, M. & Durán-Suárez, J. A. (2020), 'A review of the factors affecting the properties and performance of hemp aggregate concretes', *Journal of Building Engineering* **31**, 101323.

Talaat, A., Emad, A., Tarek, A., Masbouba, M., Essam, A. & Kohail, M. (2021), 'Factors affecting the results of concrete compression testing: A review', *Ain Shams Engineering Journal* **12**(1), 205–221.

Wittmann, X., Sadouki, H. & Wittmann, F. (1989), 'Numerical evaluation of drying test data', *Transactions 10th Int.Conf.on Struct.Mech.in Reactor Technology* pp. 71–89.

Xu, Y. & Chen, S. (2016), 'A method for modeling the damage behavior of concrete with a three-phase mesostructure', *Construction and Building Materials* **102**, 26–38.

Yang, Z., Ren, W., Sharma, R., McDonald, S., Mostafavi, M., Vertyagina, Y. & Marrow, T. (2017), 'In-situ x-ray computed tomography characterisation of 3d fracture evolution and image-based numerical homogenisation of concrete', *Cement and Concrete Composites* **75**, 74–83.

Zhou, H., Bian, H., Jia, Y. & Shao, J.-F. (2013), 'Elastoplastic damage modeling the mechanical behavior of rock-like materials considering confining pressure dependency', *Mechanics Research Communications* **53**, 1–8.

Zhou, Y., Jin, H. & Wang, B. (2020), 'Drying shrinkage crack simulation and meso-scale model of concrete repair systems', *Construction and Building Materials* **247**, 118566.